IAC-18-C1.6.13

FEASIBILITY ASSESSMENT OF AUTONOMOUS OPTICAL NAVIGATION IN LUMIO MISSION

Vittorio Franzese[1], Simone Ceccherini[2], Karthik V. Mani[3], Pierluigi Di Lizia[4], Francesco Topputo[5]

Autonomous optical navigation is one of the key enabling technologies for the Lunar Meteoroid Impacts Observer (LUMIO) mission, as well as for other deep-space science and exploration CubeSat missions. Traditional navigation techniques rely on radiometric tracking from ground stations, but a flight dynamics team must be allocated for every mission phase like in a conventional spacecraft mission, thus increasing the ground segment costs. The challenge of granting autonomy in navigation to deep-space CubeSats is faced by LUMIO, acknowledged by ESA as ex-aequo winner of SysNova Lunar CubeSats for Exploration competition, and currently under consideration for future implementation by the Agency. LUMIO envisages a 12U CubeSat form-factor placed in a halo orbit at Earth-Moon L2 to characterize the lunar meteoroid flux by detecting the impact flashes produced on the far-side of the Moon. LUMIO CubeSat performs autonomous on-board optical navigation by processing resolved images of the Moon, where its full-disk is visible. The relative position vector to the Moon is estimated by linking the Moon apparent size in an image with the real one, and the Moon position in the acquired image to the LUMIO-to-Moon line of sight, provided that both the spacecraft attitude and the Moon ephemeris are known. Then, an extended Kalman filter is exploited to estimate the spacecraft full state and increase the estimation accuracy. This work shows the performances of the full-disk autonomous optical navigation for LUMIO, and discusses improvements in view of the possible mission implementation.

1 Introduction

CubeSats' appealing is growing within the space community due to their capability of accomplishing relevant scientific and engineering tasks while still being low-cost platforms [1]. The savings in the total cost are attributable to the reduced size, mass, and power required for a CubeSat with respect to traditional spacecraft, which leads to an always increasing number of CubeSat launches per year [2]. However, navigating CubeSats with traditional techniques still requires ground facilities to perform radiometric tracking [3], thus keeping the same navigation cost of larger spacecraft. Full or partial autonomous navigation techniques would reduce the navigation cost and consequently the overall cost of space missions by leaving out or lowering the tracking from ground stations.

The Lunar Meteoroid Impacts Observer (LUMIO) is a 12U CubeSat form-factor mission to observe, quantify, and characterize the meteoroid impact flux in the Lunar environment by detecting their impact flashes on the lunar far-side [4]. LUMIO was awarded ex-aequo winner of the European Space Agency's challenge Lunar CubeSat for Exploration, under the SysNova framework. A consecutive independent assessment conducted at ESA's Concurrent Design Facility has proven the mission feasible [5]. LUMIO is located on a quasi-halo orbit about the second Lagrangian point of the Earth-Moon system [6]. This orbit allows extended imaging of the lunar far-side to gather images of the Moon for light flashes detection due to meteoroid impacts. These images, acquired by the LUMIO scientific payload (the LUMIO-Cam, an optical instrument capable of detecting faint flashes [4]), are also used to navigate autonomously using the Moon full-disk images through the Horizon-Based navigation method [7]. In this work, the performances of the autonomous horizon-based navigation for LUMIO are assessed by simulating the navigation method with synthetic Moon images and discussed in view of future mission study phases.

[1]PhD Candidate, Department of Aerospace Science and Technology, Politecnico di Milano, Via La Masa 34, 20156, Milano, Italy, vittorio.franzese@polimi.it
[2]Research Assistant, Department of Aerospace Science and Technology, Politecnico di Milano, Via La Masa 34, 20156, Milano, Italy, simone.ceccherini@polimi.it
[3]PhD Candidate, Department of Aerospace Science and Technology, Politecnico di Milano, Via La Masa 34, 20156, Milano, Italy, karthikvenkatesh.mani@polimi.it
[4]Assistant Professor, Department of Aerospace Science and Technology, Politecnico di Milano, Via La Masa 34, 20156, Milano, Italy, pierluigi.dilizia@polimi.it
[5]Assistant Professor, Department of Aerospace Science and Technology, Politecnico di Milano, Via La Masa 34, 20156, Milano, Italy; francesco.topputo@polimi.it

2 LUMIO Orbit

The particular quasi-halo orbit around the second Lagrangian point of the Earth-Moon system is shown in Figure 1. It has been derived to optimize the observation of the lunar far-side [8]. This orbit, having a Jacobi constant of 3.09 and a range to the Moon from 35525 km to 86551 km, grants the steadiness of operations since it is quasi-resonant by a factor 2:1 with the Earth-Moon system, so that LUMIO completes two revolutions every synodic period of the Earth-Moon system.

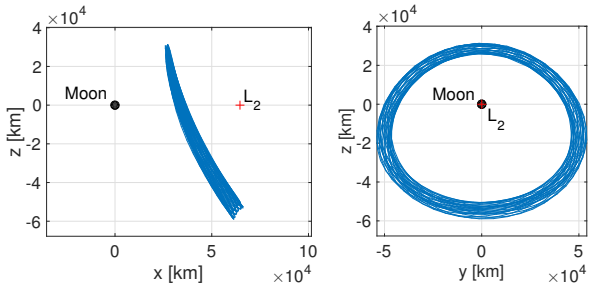

(a) Lateral view. (b) Front view.

Fig. 1: LUMIO operative orbit.

One of the two consecutive revolutions is dedicated to engineering operations (e.g., station keeping), while the other one to the LUMIO scientific investigation, that is the detection of meteoroid impacts on the lunar far-side. As shown in Figure 2, the engineering and navigation phase occurs when the Moon is seen as lit from the L2 point, while the scientific phase occurs when the lunar far-side is dark as seen from L2.

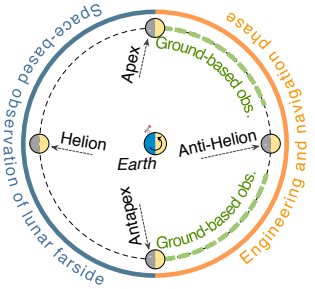

Fig. 2: LUMIO concept of operations.

A total 1-year station keeping cost of 18 m/s is required for the selected orbit [6], provided that the position and velocity vectors components are determined with an accuracy of 30 km and 50 cm/s, respectively. Three equally distributed station keeping maneuvers are planned each engineering orbit and a 30 cm/s accuracy in velocity components is required 24 hours before the maneuver execution. These are the main navigation requirements for LUMIO.

3 Horizon-based Navigation

A preliminary trade-off about different navigation techniques for the LUMIO operative orbit, such as the traditional radiometric tracking [3], the X-ray pulsar navigation [9, 10], the Celestial Triangulation [11, 12], and the Horizon-based navigation [7, 13, 14] has been performed where the figures of merit are the autonomy, the accuracy, the sensor maturity, and the cost for each navigation method. The radiometric tracking has been excluded for the purpose of granting autonomy to LUMIO and due to the inherent costs related to the use of ground stations. At the time of writing, the X-ray pulsar navigation is the most promising method for future missions, but still requires sensor development for CubeSat implementation. The Celestial Triangulation needs many celestial objects to triangulate the LUMIO position. The Horizon-Based navigation has been selected as baseline because it uses the full-disk Moon images acquired by the LUMIO-Cam to estimate the spacecraft position, thus optimizing the mass and power budgets for the navigation system and the overall cost, since no additional sensors and ground contacts are required.
Different solutions to the Horizon-based optical navigation problem for elliptical bodies of given shape matrix $A = \mathrm{diag}(a^{-2};\ b^{-2};\ c^{-2})$, where a, b, and c are the semi-axis lengths, have been proposed [7, 13, 14]. The measurements of the methods are the line-of-sight (LOS) directions to a number of horizon points retrieved from images, that are used to estimate the spacecraft position provided that attitude is known. The formulation from [7] is a simple non-iterative solution. Initially, all the LOS directions to the horizon points are expressed in the Cholesky space as

$$\boldsymbol{\rho}_{i,c} = \boldsymbol{U}\boldsymbol{\rho}_i, \tag{1}$$

where $\boldsymbol{\rho}_i$ is the LOS to the i-esimal horizon point, $\boldsymbol{U}$ is the Cholesky decomposition of the ellipsoid shape matrix $\boldsymbol{A}$, so that $\boldsymbol{A} = \boldsymbol{U}^T\boldsymbol{U}$, and $\boldsymbol{\rho}_{i,c}$ is the LOS to the i-esimal horizon point expressed in the Cholesky space. Then, all the directions $\boldsymbol{\rho}_{i,c}$ are collected in a rectangular matrix $\boldsymbol{C}$ and the vector $\boldsymbol{n}$ is estimated in least squares from

$$\boldsymbol{C}\,\boldsymbol{n} = \mathbf{1}_m, \tag{2}$$

where m is the number of measured horizon points and $\mathbf{1}_m$ is a column vector of size m where each component is 1. Once obtained n, the camera-to-object position vector $\boldsymbol{r}$ is estimated as

$$\boldsymbol{r} = -\,\boldsymbol{U}^{-1}\,(\boldsymbol{n}^T\,\boldsymbol{n} - 1)^{-1/2}\,\boldsymbol{n}. \tag{3}$$

4 Simulation Setup

The simulation of the proposed horizon-based autonomous optical navigation for LUMIO and the assessment of its performances are structured in different steps, which span from the generation of synthetic images to the spacecraft state estimation. In particular, three macro-sections are defined, which are the:
- Generation of synthetic Moon images (Section 4.1);
- Processing of Moon images (Section 4.2);
- Spacecraft Orbit Determination (Section 4.3).
These phases are described hereinafter.

4.1 Image generation

The generation of synthetic Moon images is accomplished by a synergy between MATLAB®and POV-Ray software. The LUMIO position in the operative orbit, together with its attitude, the LUMIO-Cam pointing direction, and the illumination geometry are retrieved from dedicated kernels at each epoch in MATLAB®. These data are sent to POV-Ray, where the LUMIO-Cam properties [8] and the Moon model with its texture and digital elevation model are defined. Then, the POV-Ray software renders synthetic Moon images for each selected epoch.

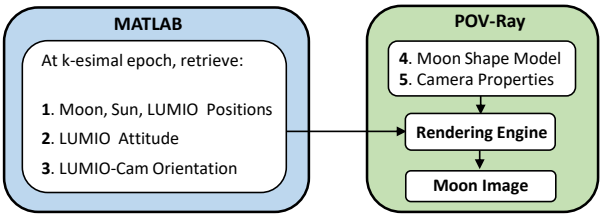

Fig. 3: Simulator architecture. The observation geometry is defined in MATLAB, while the optical and shape properties in POV-Ray.

4.2 Image Processing

The aim of the image processing is to detect the pixels belonging to the Moon lit horizon and fit an ellipse to these points, so estimating the Moon apparent disk [11, 13], as shown in Figure 4. This is achieved through the following steps [7]:
1) Image acquisition and correction;
2) Black and white conversion;
3) Estimation of light direction;
4) Edge finding methods application (e.g., Canny [15]);
5) Selection of lit horizon line;
6) Ellipse fitting to horizon pixels.
The ellipse fitted to the horizon points is an estimation of the Moon full disk. The LOS directions to the Moon disk ($\boldsymbol{\rho}_i$) can then be retrieved from the the image and used to estimate the spacecraft position as per Section 3. For the sake of clarity, other image processing algorithms to estimate an object full disk exist [14, 16].

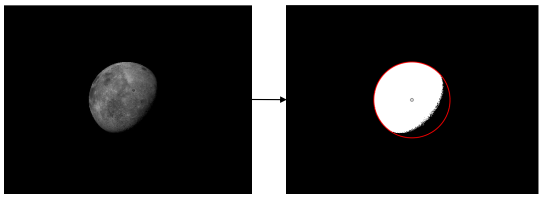

Fig. 4: Moon full disk estimation.

4.3 Orbit Determination

An extended Kalman filter [17] has been implemented to increase the position estimation accuracy and to provide a velocity estimate. The output from the procedure in Section 3 is the CubeSat position vector in the camera reference frame, which can be expressed into the J2000 reference frame centered at the Moon through the attitude matrix (assumed to be known) and the camera relative position and attitude kernels. The system equations are then

$$\boldsymbol{x}_k = \boldsymbol{f}(\boldsymbol{x}_{k-1}, \boldsymbol{w}_{k-1}), \tag{4}$$

$$\boldsymbol{y}_k = \boldsymbol{H}\,\boldsymbol{x}_k + \boldsymbol{v}_k, \tag{5}$$

where $\boldsymbol{x}$ is the 6x1 spacecraft state vector expressed in the J2000 reference frame centered at the Moon, $\boldsymbol{f}$ is the right-hand side of the astrodynamics model [18], $\boldsymbol{y}$ is the 3x1 camera-to-Moon position measurement expressed in the J2000 frame, $\boldsymbol{H} = [\boldsymbol{I}_{3x3}; \boldsymbol{0}_{3x3}]$, and k is the discrete step. The model and measurement errors, $\boldsymbol{w}$ and $\boldsymbol{v}$, respectively, are mutually uncorrelated zero-mean white noise processes with known covariances ($\boldsymbol{Q}$ and $\boldsymbol{R}$, respectively),

$$\boldsymbol{w}_k \sim (\boldsymbol{0},\, \boldsymbol{Q}_k), \tag{6}$$

$$\boldsymbol{v}_k \sim (\boldsymbol{0},\, \boldsymbol{R}_k). \tag{7}$$

At each k, the prediction step is

$$\hat{\boldsymbol{x}}_k^- = \boldsymbol{f}(\hat{\boldsymbol{x}}_{k-1}^+), \tag{8}$$

$$\boldsymbol{P}_k^- = \boldsymbol{F}_{k-1}\boldsymbol{P}_{k-1}^+\boldsymbol{F}_{k-1}^T + \boldsymbol{Q}_{k-1}, \tag{9}$$

while the correction step is

$$\boldsymbol{K}_k = \boldsymbol{P}_k^-\,\boldsymbol{H}^T(\boldsymbol{H}\,\boldsymbol{P}_k^-\,\boldsymbol{H}^T + \boldsymbol{R}_k)^{-1}, \tag{10}$$

$$\hat{\boldsymbol{x}}_k^+ = \hat{\boldsymbol{x}}_k^- + \boldsymbol{K}_k\,[\boldsymbol{y}_k - \boldsymbol{H}\,\hat{\boldsymbol{x}}_k^-], \tag{11}$$

$$\boldsymbol{P}_k^+ = (\boldsymbol{I} - \boldsymbol{K}_k\,\boldsymbol{H})\,\boldsymbol{P}_k^-, \tag{12}$$

where $\boldsymbol{P}$ is the state estimate error covariance, $\boldsymbol{F}$ is $\partial\boldsymbol{f}/\partial\boldsymbol{x}$, $\boldsymbol{K}$ is the Kalman gain, the "$\wedge$" superscript denotes estimated quantities, and "-" and "+" denote predicted and corrected variables, respectively.

5 Navigation Performances

5.1 Error Template

The methods outlined in Section 3 and Section 4.2 have been applied to the synthetic Moon images to retrieve a static error template. This template, shown in Figure 5, is used to characterize the error in the Kalman filter.

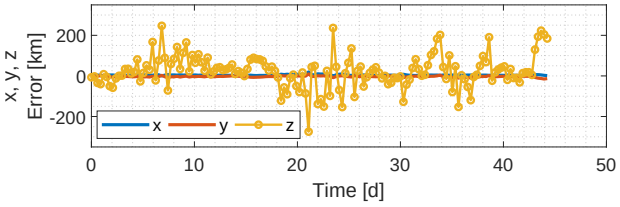

Fig. 5: Static error template during three halo periods.

The error in Figure 5 is computed in the camera reference frame, where x, y, and z are the left, up, and depth directions, respectively. The maximum root mean squared error (RMSE) of this template, defined as:

$$\text{RMSE} = \sqrt{\frac{\sum_{i=1}^{N} p_i^2}{N}}, \tag{13}$$

where p_i is the error of one position component at the epoch i and N is the total number of measurements, is RMSE = 83.60 km, and is used to characterize the standard deviation of the white noise processes in the Kalman filter.

5.2 Frequency Tuning

LUMIO executes three station keeping maneuvers and requires a state vector knowledge accuracy of 30 km in position components and 30 cm/s in velocity components 24 hours before the maneuver execution (cut-off time) during the engineering orbits, as shown in Figure 6(a), where three halo orbit periods are presented (the first and the third orbit period are those devoted to engineering and navigation). The frequency in acquiring images is increased before the cut-off time to provide better inputs to the Kalman filter.
The following acquisition frequencies are used throughout the halo orbits:
1) A High Frequency of 1 acquisition per minute (HF = 16.7 mHz) starting one day before the cut-off times;
2) A Medium Frequency of 1 acquisition per 10 minutes (MF = 1.67 mHz) is during nominal operations;
3) A Low Frequency of 1 acquisition per 60 minutes (LF = 0.277 mHz) during scientific operations.

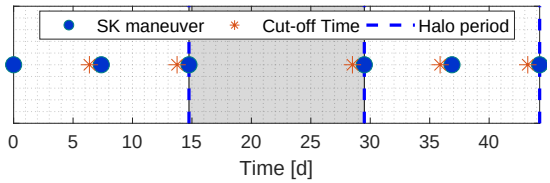

(a) Station Keeping maneuvers planning.

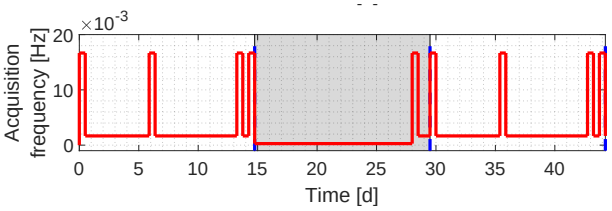

(b) Acquisition frequency planning.

Fig. 6: LUMIO Concept of operations for station keeping. (a) Planning of S/K maneuvers; (b) Modulation of acquisition frequency to meet navigation requirements. The shaded zone is related to the science orbit where no S/K is planned.

5.3 Filter Settings

The measurements of the extended Kalman filter are zero-mean white noise processes with a 3σ standard deviation of 250.8 km assigned to each position vector component (X, Y, and Z). This follows the error characterization in Section 5.1. The initial state covariance $\boldsymbol{P}_0$ is

$$\boldsymbol{P}_0 = \begin{bmatrix} 10^4\,\boldsymbol{I}_3 & \boldsymbol{0}_3 \\ \boldsymbol{0}_3 & 10^{-6}\,\boldsymbol{I}_3 \end{bmatrix}, \tag{14}$$

while the process noise covariance and the measurement noise covariance are

$$\boldsymbol{Q} = \begin{bmatrix} 10^{-12}\,\boldsymbol{I}_3 & \boldsymbol{0}_3 \\ \boldsymbol{0}_3 & 10^{-12}\,\boldsymbol{I}_3 \end{bmatrix}, \tag{15}$$

$$\boldsymbol{R} = 7 \times 10^3\,\boldsymbol{I}_3, \tag{16}$$

where units of km^2 are used for position-related quantities and km^2/s^2 for velocity-related quantities.

5.4 Filter Outputs

The 3σ covariance bounds in terms of position and velocity components estimation as output of the Kalman filter are shown in Figure 7. The dashed vertical lines delimit the three halo periods, where the first and the third periods are related to the engineering orbit, and the second period to the science orbit. The position and velocity errors are always kept within 30 km and 50 cm/s during engineering operations, with a refinement on the velocity estimation at the cut-off time for the station keeping maneuvers, as discussed in Section 2.

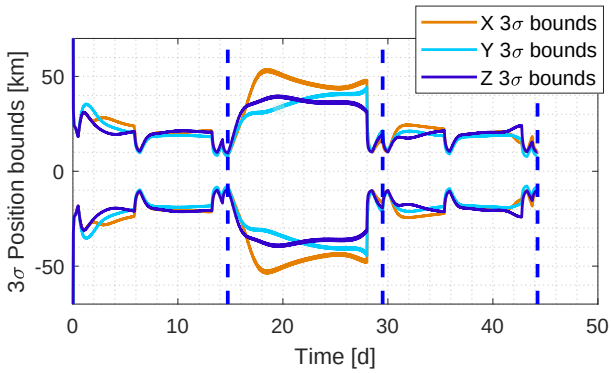

(a) 3σ covariance Bounds in position components estimation.

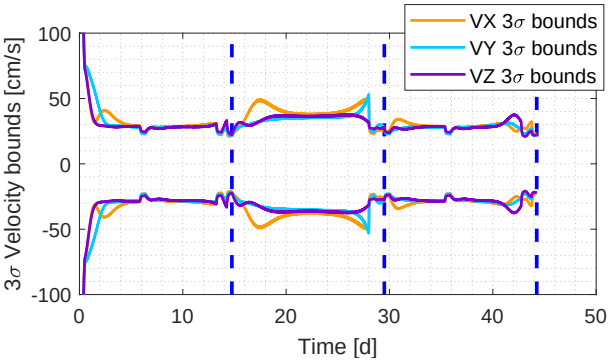

(b) 3σ covariance bounds in velocity components estimation.

Fig. 7: 3σ covariance bounds in (a) position and (b) velocity components estimation.

6 Conclusions

The feasibility of horizon-based autonomous optical navigation using Moon images for LUMIO, a CubeSat form-factor mission at the second Lagrangian point of the Earth–Moon system, has been investigated. Synthetic images of the Moon have been generated by a combination of MATLAB®and POV-Ray and processed to estimate the spacecraft position and its full state through an extended Kalman filter. The results in terms of position and velocity components estimation bounds confirm the preliminary feasibility of autonomous optical navigation for the LUMIO mission.

Acknowledgments

Part of this work has been conducted under ESA Contract No. 4000120225/17/NL/GLC/as. The authors would like to acknowledge Roger Walker and Johan Vennekens for their support. The authors would also like to acknowledge the members of the LUMIO team for their contributions.

Bibliography

[1] R. Walker et al. A hitchhikers guide to the solar system: future missions of deepspace nanospacecraft. In *4S Symposium*, 2018.

[2] A. Poghosyan and A. Golkar. CubeSat evolution: Analyzing CubeSat capabilities for conducting science missions. *Progress in Aerospace Sciences*, 88:59–83, 2017. doi: 10.1016/j.paerosci.2016.11.002.

[3] C. L. Thornton and J. S. Border. *Radiometric Tracking Techniques for Deep Space Navigation*, chapter 2. John Wiley & Sons, 2003. doi: 10.1002/0471728454.

[4] F. Topputo, M. Massari, J. Biggs, et al. LUMIO: a Cubesat at Earth-Moon L2. In *4S Symposium*, pages 1–15, 2018. handle: 11311/1055454.

[5] CDF Team. CDF Study Report: LUMIO. Review of SysNova Award LUMIO Study. Technical report, European Space Research and Technology Centre, ESA, 2018.

[6] S. Speretta, F. Topputo, et al. LUMIO: achieving autonomous operations for Lunar exploration with a CubeSat. In *2018 SpaceOps Conference*, page 2599, 2018. doi: 10.2514/6.2018-2599.

[7] J. A. Christian and S. B. Robinson. Noniterative Horizon-Based Optical Navigation by Cholesky Factorization. *Journal of Guidance, Control, and Dynamics*, 39(12):2757–2765, 2016. doi: 10.2514/1.G000539.

[8] A. Cipriano, D. A. Dei Tos, and F. Topputo. Orbit Design for LUMIO: the Lunar Meteoroid Impacts Observer. *Frontiers in Astronomy and Space Sciences*, 5:29, 2018. doi: 10.3389/fspas.2018.00029.

[9] S. I. Sheikh, D. J. Pines, Paul S. Ray, et al. Spacecraft Navigation Using X-Ray Pulsars. *Journal of Guidance, Control, and Dynamics*, 29(1):49–63, 2006. doi: 10.2514/1.13331.

[10] K.D. Anderson, D.J. Pines, and S.I. Sheikh. Validation of pulsar phase tracking for spacecraft navigation. *Journal of Guidance, Control, and Dynamics*, 38(10):1885–1897, 2015. doi: 10.2514/1.G000789.

[11] D. Mortari and D. Conway. Single-point position estimation in interplanetary trajectories using star trackers. *Advances in the Astronautical Sciences*, 156(1):1909–1926, 2016. doi: 10.1007/s10569-016-9738-4.

[12] R. Karimi and D. Mortari. Interplanetary Autonomous Navigation Using Visible Planets. *Journal of Guidance, Control, and Dynamics*, 38(6):1151–1156, 2015. doi: 10.2514/1.G000575.

[13] J. A. Christian. Optical Navigation Using Iterative Horizon Reprojection. *Journal of Guidance, Control, and Dynamics*, 39(5):1092–1103, 2016. doi: 10.2514/1.G001569.

[14] D. Mortari, C. N. D'Souza, and R. Zanetti. Image processing of illuminated ellipsoid. *Journal of Spacecraft and Rockets*, pages 448–456, 2016. doi: 10.2514/1.A33342.

[15] Canny J. A Computational Approach to Edge Detection. *IEEE Transactions on Pattern Analysis and Machine Intelligence*, pages 679–689, 1986. doi: 10.1109/TPAMI.1986.4767851.

[16] J. A. Christian. Accurate planetary limb localization for image-based spacecraft navigation. *Journal of Spacecraft and Rockets*, 54(3):708–730, 2017. doi: 10.2514/1.A33692.

[17] D. Simon. *Optimal state estimation: Kalman, H infinity, and nonlinear approaches*, chapter 13. John Wiley & Sons, 2006. doi: 10.1002/0470045345.

[18] D. A. Dei Tos and F. Topputo. Trajectory refinement of three-body orbits in the real solar system model. *Advances in Space Research*, 59(8):2117–2132, 2017. doi: 10.1016/j.asr.2017.01.039.